

Pleistocene shifts in Great Basin hydroclimate seasonality govern the formation of lithium-rich paleolake deposits

Tripti Bhattacharya,^{1*} Peter Brennan,¹ Daniel E. Ibarra,²
Catherine A. Gagnon,² Kristina L. Butler,^{2,3} Alexa Terrazas,⁴ Shaw Miller,
² Lee Ann Munk,⁵ David F. Boutt,⁶ Ran Feng,⁷
Stephanie N Bullinger,¹ Lucy Weisbeck¹

¹Department of Earth and Environmental Sciences, Syracuse University, Syracuse NY

²Department of Earth, Environmental, and Planetary Sciences, Brown University, Providence, RI

³Department of Sustainable Earth Systems Sciences, University of Texas at Dallas, Dallas TX

⁴Department of Atmospheric and Oceanic Sciences, University of California Los Angeles, Los Angeles CA

⁵Department of Geological Sciences, University of Alaska-Anchorage, Anchorage AK

⁶Department of Geosciences, University of Massachusetts-Amherst, Amherst, MA

⁷Department of Earth, Geographic, and Climate Sciences, University of Connecticut, Storrs CT

*To whom correspondence should be addressed; E-mail: trbhata@syr.edu.

This paper is a non-peer reviewed preprint submitted to EarthArXiv. It will be updated as the manuscript progresses through peer review.

1 Highlights

2 **Pleistocene shifts in Great Basin hydroclimate seasonality govern the forma-** 3 **tion of lithium-rich paleolake deposits**

4 Tripti Bhattacharya, Peter R. Brennan, Daniel E. Ibarra, Catherine A. Gagnon,
5 Kristina L. Butler, Alexa Terrazas, Shaw Miller, Lee Ann Munk, David F. Boutt,
6 Ran Feng, Stephanie N. Bullinger, Lucy Weisbeck

- 7 • Leaf wax hydrogen isotopes from the Plio-Pleistocene southern Great Basin
8 reveal a reduction in winter rainfall between 2.6 and 2.2 Ma
- 9 • Early Pleistocene fluctuations in winter rainfall were likely driven by shifts
10 in the meridional sea surface temperature gradient in the Pacific
- 11 • Shifts in past hydroclimate likely played an integral role in the formation of
12 lithium-rich lacustrine clay deposits in western North America

13 Pleistocene shifts in Great Basin hydroclimate
14 seasonality govern the formation of lithium-rich
15 paleolake deposits

16 Tripti Bhattacharya^a, Peter R. Brennan^a, Daniel E. Ibarra^b, Catherine A.
17 Gagnon^b, Kristina L. Butler^{b,d}, Alexa Terrazas^c, Shaw Miller^b, Lee Ann Munk^e,
18 David F. Boutt^f, Ran Feng^g, Stephanie N. Bullinger^a, Lucy Weisbeck^a

^a*Department of Earth and Environmental Sciences, Syracuse University,*

^b*Department of Earth, Environmental and Planetary Science, Brown University,*

^c*Department of Atmospheric and Oceanic Sciences, University of California Los Angeles,*

^d*Department of Sustainable Earth Systems Sciences, The University of Texas at Dallas,*

^e*Department of Geological Sciences, University of Alaska-Anchorage,*

^f*Department of Geosciences, University of Massachusetts-Amherst,*

^g*Department of Earth, Geographic, and Climate Sciences, University of Connecticut,*

19 **Abstract**

Southwestern North America is currently experiencing a multidecadal megadrought, with severe consequences for water resources. However, significant uncertainty remains about how precipitation will change in the 21st century in this semi-arid region. Paleoclimatic records are essential for both contextualizing current change, and for helping constrain the sensitivity of regional hydroclimate to large-scale global climate. In this paper, we present a new 2.8 Ma late Pliocene to present compound-specific isotopic record from Clayton Valley, the site of a long-lived paleolake in the southern Great Basin. Hydrogen and carbon isotopes from terrestrial plant leaf waxes provide evidence of past shifts in rainfall seasonality as well as ecosystem structure, and help contextualize the formation of this lithium-rich lacustrine basin. Our results suggest that regional hydroclimates underwent

a substantial reorganization at the Plio-Pleistocene boundary, especially between 2.6 and 2.0 Ma. In this interval, a reduced latitudinal temperature gradient in the North Pacific likely resulted in a northward shift in storm tracks, and a reduction in winter rainfall over the southern Great Basin. This occurred against a background of increased summer rainfall and a greater accumulation of lithium in the lake basin. Our interpretation is corroborated by a compilation of Plio-Pleistocene north Pacific sea surface temperature records, as well as an isotope-enabled model simulation. Overall, these results suggest that past shifts in rainfall seasonality helped set the stage for the development and dessication of lithium-rich lacustrine deposits.

20 *Keywords:* Plio-Pleistocene, southwest North America

21 *PACS:* 0000, 1111

22 *2000 MSC:* 0000, 1111

23 **1. Introduction**

24 Southwestern North America is currently in the midst of an ongoing megadrought
25 that has resulted in reductions in water resources, snowpack, and an increase in
26 related hazards like wildfire. Although megadroughts have occurred in this re-
27 gion historically, anthropogenic emissions have likely exacerbated the risk of 21st
28 century megadrought (Williams et al., 2020). While increases in temperature
29 play a key role in increasing 21st century drought (King et al., 2024), rainfall
30 remains much more uncertain. Southwestern North America features a bimodal
31 rainfall distribution: the region receives rainfall from the North American Mon-

32 soon (NAM) in summer, while midlatitude storms provide rainfall in the winter.
33 The future behavior and relative contribution of both these precipitation regimes
34 remains unclear (Choi et al., 2016; Almazroui et al., 2021). State-of-the-art Earth
35 System Models (ESMs) disagree about the future response of the NAM to anthro-
36 pogenic warming, which may result from models' persistent sea surface tempera-
37 ture (SSTs) biases in the North Pacific, as well as the inability of coarse-resolution
38 models to resolve the details of moist convection associated with the monsoon
39 (Cook and Seager, 2013; Pascale et al., 2017; Almazroui et al., 2021; Wallace and
40 Minder, 2024). Similarly, model disagreement about the future behavior of win-
41 ter precipitation stems in part from model disagreement about future large-scale
42 changes in circulation over the North Pacific (Choi et al., 2016).

43
44 In the face of this uncertainty, paleoclimatic data can help constrain the sensi-
45 tivity of southwest hydroclimates to large-scale climate forcings. Evidence from
46 past greenhouse climates, including the Pliocene, the last interval in Earth his-
47 tory when CO₂ was above pre-industrial levels, has helped constrain the response
48 of southwestern hydroclimates to a warmer background climate state. Proxy ev-
49 idence from the Pliocene suggests that the NAM was stronger between 3.5 and
50 roughly 2.0 Ma, and could have contributed to increased lake levels and more
51 mesic vegetation in the southwest (Bhattacharya et al., 2022). Modeling experi-
52 ments with Pliocene boundary conditions have also helped clarify how other phe-
53 nomena like atmospheric rivers respond to changes in topography and geography,
54 as well as altered SST patterns (Menemenlis et al., 2021; Brennan et al., 2022).

55 However, while there is some suggestion that long-term changes in winter storms
56 could have driven higher lake levels in the Pliocene, it remains unclear how win-
57 ter storm tracks over the eastern Pacific and western North America responded
58 to global cooling over the Plio-Pleistocene transition (Ibarra et al., 2018; Peale
59 et al., 2024).

60

61 Here, we present new evidence of late Pliocene and early Quaternary hydro-
62 climate shifts recorded in lake sediments from Clayton Valley, a paleolake basin
63 in Nevada that is currently the site of a lithium brine operation. Understanding the
64 evolution of this lake basin therefore has the potential to shed light on the environ-
65 mental conditions that help concentrate lithium, an element critical to the energy
66 transition, in sedimentary environments such as Clayton Valley and other loca-
67 tions (Vine, 1975; Davis et al., 1986; Gagnon et al., 2023; Benson et al., 2023).
68 We present new stable hydrogen and carbon isotopes in long-chain terrestrially de-
69 rived leaf waxes in a sediment core that spans the interval from the late Pliocene,
70 2.8 Ma, and continues until the present-day.

71 Previous geochemical data has helped clarify the history of aridity in this
72 basin, as well as how climate contributed to the formation of lithium-rich clays
73 in the basin (Coffey et al., 2021; Gagnon et al., 2023). However, leaf wax iso-
74 topes provide a novel perspective, since hydrogen isotopes in these long-chain
75 alkyl compounds have been shown to have a strong correlation with the hydro-
76 gen isotopic composition of precipitation, while carbon isotopes reflect large-
77 scale ecosystem structure (Sachse et al., 2012; Inglis et al., 2022). We there-

78 fore use these data to assess how changes in winter storms, or summertime mois-
79 ture, contributed to the evolution of hydroclimate at Clayton Valley over the Plio-
80 Pleistocene transition. This allows us to test if precipitation seasonality changes
81 may have influenced lithium delivery, via weathering and solute generation and
82 concentrating processes to the paleolake. We complement these data with anal-
83 ysis of previously published regional sea surface temperature records as well as
84 climate model simulations in order to evaluate the large-scale controls on changes
85 in hydroclimate in the desert southwest.

86 **2. Background and Methods**

87 *2.1. Geological and Climatological Setting*

88 Clayton Valley (CV) is a topographically closed, half-graben basin in the
89 Basin and Range Province (Vine, 1975; Davis et al., 1986; Coffey et al., 2021;
90 Gagnon et al., 2023) (Figure 1). Currently, the basin is a source of lithium (Li)
91 from brines rich in the element (Munk et al., 2016). The Clayton Valley playa
92 sits at an elevation of 1400 masl, and is 30 km to the northwest of Death Valley.
93 Although much of the uplift in this region occurred prior to the early Pliocene,
94 evidence suggests that the elevation ranges of nearby mountain ranges, includ-
95 ing the central Sierra Nevada were established between 1 and 3 Ma, creating a
96 rainshadow to the west of CV (Thompson, 1991; Mix et al., 2019). Currently,
97 vegetation in the valley consists of sparse sagebrush (*Artemisia* spp.) and cre-
98 osote (*Larrea* spp.), with nearby mountain regions contain a mix of oak (*Quercus*
99 spp.), juniper (*Juniperus* spp.), and other conifers. While potential evapotranspi-

100 ration exceeds precipitation in the southern Great Basin, the region does receive
101 roughly 13 cm of rainfall a year (Munk and Chamberlain, 2011).

102

103 Rainfall in CV derives from two distinct seasonal sources. The valley receives
104 the majority of its rainfall in winter, when the jet over the eastern Pacific steers
105 storms towards the west coast of North America (Gagnon et al., 2023). However,
106 approximately 20-30% of annual rainfall at CV also derives from the summer
107 monsoon, when surges of monsoonal moisture from the south extend into regions
108 of the southern Great Basin (Bhattacharya et al., 2023). These sources of mois-
109 ture have distinct isotopic signals: a nearby isotope monitoring station reveals that
110 summertime rainfall has a hydrogen isotopic value of roughly -50‰ , while win-
111 ter rainfall is closer to -100‰ . The relative enrichment of summer compared to
112 winter rainfall is well documented in other sources (Eastoe and Dettman, 2016;
113 Aggarwal et al., 2016; Bhattacharya et al., 2018, 2022). The complex topography
114 of the Sierra Nevada blocks atmospheric circulation, resulting in site by site vari-
115 ations in the relative proportions of summer or winter moisture that reach leeward
116 sites like CV (Lechler and Galewsky, 2013).

117

118 2.2. *Sedimentology and Age Model*

119 Drill core EXP2 was drilled between June and November 2017 by commer-
120 cial Li mining operation (Albemarle Corporation) in the CV basin. The core is
121 990.6 m in length, and detailed information on the sedimentology of the core, as

122 well as its environmental interpretation, is available in Gagnon et al. (2023) and
123 Coffey et al. (2021). The upper 228.6 m of the core consists of sands and gravels,
124 transitioning to clays with thin infrequent sand layers in the lower part of the unit.
125 Between 228.6 and 405 m, the EXP2 core consists of brown and green clays with
126 layers of silty clays and silty clay. Between 405.4 to 535.0 m, the core contains
127 thick layers of halite interbedded with thin layers of clay. Between 535.0 and
128 896.7 m, the unit contains green clay and thin volcanic ash layers. Below this,
129 the core consists of angular gravel with siltstone clasts, with a lithic tuff at the
130 base of the core. Prior work inferred the existence of a deep lake between 896.7
131 m and 535 m, with dessication occurring between 535 and 405 m, followed by the
132 existence of a shallow lake (Gagnon et al., 2023). Details of stratigraphy are pro-
133 vided in Gagnon et al. (2023). The age model for the site is based on 5 previously
134 published argon-argon dates from sanidine/plagioclase as well as a zircon U-Pb
135 age (Coffey et al., 2021; Gagnon et al., 2023). The age model was constructed us-
136 ing Bayesian age modeling techniques following Blaauw et al. (2018) in Gagnon
137 et al. (2023), and reveals a relatively constant accumulation rate over the record.
138 Unfortunately, the EXP2 drill core only provides a continuous record back to 2.8
139 Ma, and therefore the records we present do not overlap with the mid-Pliocene or
140 mid-Piacenzian warm period, an interval between roughly 3.3 and 3.0 Ma that has
141 been the target of paleoenvironmental reconstruction. However, the core from this
142 site does provide a unique view of the Plio-Pleistocene transition from the interior
143 of southwestern North America.

144 2.3. *Leaf Wax Analyses*

145 Leaf waxes were extracted using standard protocols. This involved an initial
146 step of sediment lyophilization, homogenization, and extraction of the total lipids
147 using an accelerated solvent extractor (ASE 350, Dionex). Our analyses focus
148 on leaf wax fatty acids, which were eluted using a mix of dichloromethane and
149 isopropanol, and then using a 5% acetic acid in dichloromethane solution over
150 aminopropyl gel. To eliminate exchangeable hydrogen in the molecule, leaf wax
151 n-acids were methylated using a methanol standard of known isotopic composi-
152 tion to create fatty acid methyl esters (FAMES). Concentrations of fatty acids were
153 determined using a Trace 1310 GC-FID. These data were also used to calculate the
154 Carbon Preference Index (CPI) and the Average Chain Length (ACL). CPI mea-
155 sures the extent to which fatty acids maintain an even-over-odd preference, and
156 values above 1 indicate a dominantly terrestrial, primary rather than petrogenic
157 source for wax compounds, while ACL represents a concentration-weighted aver-
158 age chain length of the wax compounds found in a sample.

159

160 We quantified the hydrogen and carbon isotopic composition of the three most
161 abundant long chain FAMES (C_{26} ; C_{28} ; and C_{30}) via gas chromatograph - isotope
162 ratio mass spectrometry (GC-IR-MS). This consists of a Thermo Delta V Plus
163 mass spectrometer coupled to a Trace 1310 GC-FID, using either a pyrolysis (H_2)
164 or combustion reactor (CO_2). H_2 and CO_2 gases calibrated to a *n*-alkane standard
165 (A7 mix provided by Arndt Schimmelmann at Indiana University) provided refer-
166 ences for each analysis. An internal isotopic standard consisting of a synthetic mix

167 of FAMEs was analyzed every 5-7 samples to monitor (and subsequently correct
168 for) instrument drift. Samples were run in triplicate for δD to obtain a precision
169 better than 2‰ (1σ), and in duplicate or triplicate for $\delta^{13}C$ to obtain a precision
170 better than 0.2‰ (1σ). Over the course of the run, precision for internal standard
171 measurements was similarly 2‰ (1σ) for hydrogen and 0.2‰ (1σ) for carbon.
172 Leaf wax values are not corrected for ice volume changes (Schrag et al., 1996;
173 Lisiecki and Raymo, 2005; Westerhold et al., 2020) to remain consistent with pre-
174 vious Plio-Pleistocene leaf wax studies in the region (Bhattacharya et al., 2022;
175 Peale et al., 2024).

176 2.4. *Inferring δD of Precipitation*

177 δD_{wax} values are generally offset from the isotopic value of environmental
178 waters or mean annual precipitation or δD_p . ε_{p-w} , otherwise known as apparent
179 fractionation, is known to vary systematically across plant clades. Graminoids
180 (e.g. grasses) have a larger ε_{p-w} (e.g. are more depleted relative to δD_p), than
181 eudicots, which likely reflects differences in leaf wax biosynthesis and leaf de-
182 velopment (Gao et al., 2014). Following our previous work (e.g. (Bhattacharya
183 et al., 2022, 2018), we use a Bayesian mixing model and $\delta^{13}C_{wax}$ data to infer the
184 proportion of waxes in a sample that derive from C_4 grasses, since C_4 plants have
185 a more enriched carbon isotopic signature than C_3 plants (Collister et al., 1994).
186 End-member constraints on C_4 grasses and C_3 eudicots come from modern plant
187 waxes included in previously published compilations (Sachse et al., 2012; Liu and
188 An, 2020). Because these constraints are primarily available for the longest chain

189 length (e.g. the C₂₉ alkane and the C₃₀ n-acid), we infer δD_p from the hydrogen
190 isotopic signature of the C₃₀ n-acid.

191 We then use the proportion of inferred C₄ vegetation to determine the appropri-
192 ate ε_{p-w} to apply to a given sample. Constraints on ε_{p-w} are obtained from δD_{wax}
193 measured on the Arizona-Sonora Desert Museum modern plants. The approach
194 involves weighting the value of ε_{p-w} for C₃ and C₄ plants by the inferred fraction
195 of C₃ and C₄ plants in the sample. Because all calculations are performed in a
196 Bayesian framework, uncertainties are propagated through all steps of the calcula-
197 tion. While our initial 1σ precision for δD_w measurements is 2‰, 1σ uncertainty
198 for our final estimate of δD_p is 5-6‰. This Bayesian approach has been previ-
199 ously used to study paleohydrological signals in leaf waxes (Tierney et al., 2017;
200 Windler et al., 2023), including within the NAM domain (Bhattacharya et al.,
201 2018, 2022). After inferring Plio-Pleistocene changes in δD_p from the C₃₀, we
202 compare these results to previously published leaf wax hydrogen isotope records
203 from the desert southwest.

204 2.5. Carbonate Isotopes and Bulk Lithium Concentrations

205 135 new carbonate oxygen and carbon isotope measurements, as well as 36
206 new lithium concentration measurements, are reported in this work. These data
207 extend the record presented in Gagnon et al. (2023) and Coffey et al. (2021).
208 For carbonate oxygen and carbon analyses, bulk core samples were homogenized
209 using a ceramic mortar and pestle and reacted with 70°C phosphoric acid un-
210 der vacuum using a Kiel IV carbonate device with the evolved carbon dioxide

211 measured on a Thermo Scientific 253 Plus 10 kV Isotope Ratio Mass Spectrom-
212 eter (Gagnon et al., 2023). External precision (1σ) for both $\delta^{18}\text{O}_w$ and $\delta^{13}\text{C}_w$
213 was $<0.1 \text{‰}$ based on repeat measurements of two internal marble standards were
214 calibrated against international recognized standards (Gagnon et al., 2023). For
215 lithium measurements, as in previous work (Gagnon et al., 2023; Coffey et al.,
216 2021), whole-rock samples were analyzed by SGS Environmental Services by
217 inductively coupled plasma-optical emission spectrometry (ICP-OES). In brief,
218 0.1g of crushed and dried sample was fused using Na_2O_2 and digested in HCl.
219 The digested solution was analyzed on an Agilent ICP-OES. The core samples
220 measured for new lithium concentrations are paired to newly reported (n=11) or
221 previously reported (n=25) measured carbonate oxygen and carbon isotope mea-
222 surements. New carbonate isotope and lithium data confirm the overall trends
223 presented in prior work, largely confirming the temporal pacing of wet and dry
224 intervals presented in Gagnon et al. (2023).

225 **3. Results**

226 *3.1. Leaf Wax Results*

227 CV EXP2 leaf waxes show remarkably stable CPI and ACL values, and indi-
228 cate limited alteration of terrestrially-derived waxes. CPI values are consistently
229 above 3, indicating a predominantly even-over-odd preference for leaf wax fatty
230 acids, suggesting a terrestrial rather than petrogenic source (Figure S1). ACL val-
231 ues are also very stable over the record, and consistently range between 26 and
232 28, indicating that long-chain waxes dominate the sample. Based on these results,

233 we analyze the carbon and hydrogen isotopic composition of three chain lengths
234 of n-acid (C_{26} ; C_{28} ; and C_{30}).

235

236 The carbon isotopic composition of all three chain lengths are strongly corre-
237 lated (Table S1). For all three chain lengths, carbon isotopic values vary between
238 approximately -30 and -24‰ VPDB (Figure 2). Between 3 and 2 Ma, the car-
239 bon isotopic signature of C_{26} , C_{28} , and C_{30} becomes more positive, increasing
240 to roughly -25‰ from -29‰ . After this point, values remain relatively sta-
241 ble, fluctuating near -24‰ until 0.5 Ma, after which they show higher amplitude
242 fluctuations.

243

244 Similar to carbon, the δD signature of all three chain lengths are strongly cor-
245 related (Table S1), and show similar long-term trends over the Plio-Pleistocene
246 transition. Between 2.8 and 2.5 Ma, all chain lengths exhibit a shift towards more
247 positive δD values, peaking at roughly 2.3 Ma, before declining by 2 Ma (Fig-
248 ure 2). This excursion is much more pronounced in the C_{26} n-acid compared to
249 C_{28} and C_{30} . This excursion to more positive values is evident in the oxygen iso-
250 tope values of authigenic carbonates from EXP2 and coincides with an increase
251 in the concentration of lithium in bulk sediments (Gagnon et al., 2023). Li con-
252 centrations peak at 2.5 Ma, and then decline by 2.0 Ma, similar to the timing of
253 the shift in carbonate and leaf wax isotopic values. After roughly 1.5 Ma, values
254 of each leaf wax fluctuate between -160 and -180‰ . We note that C_{26} is slightly
255 more enriched in deuterium than the other two chain lengths of n-acid (Figure 2).

256

257 The CV EXP2 δD_p record, inferred from the C_{30} acidm fluctuates between -60
258 and -100‰ VSMOW, apart from one basal outlying value (Figure 4). The most
259 modern values are between -80 and -100‰ VSMOW, similar to modern winter
260 values of δD_p from the NV-00 station (Figure 1, 4). This observation increases
261 our confidence that our approach to reconstructing δD_p , especially our choice of
262 ε_{p-w} , yields reasonable results. We compare the EXP2 δD_p reconstruction to two
263 other continuous Plio-Pleistocene leaf wax records from the southwest that both
264 extend back to 3.5 Ma (Figure 3). We note that the leaf wax-inferred δD_p record
265 from CV exhibits some similar features to the two available leaf wax records from
266 the region from ODP 1012 on the southern California margin and DSDP 475 off
267 Baja California. Notably, all three records show a decline in δD_p between 2.9 and
268 2.75 Ma and all three records show slightly more positive values between 2.6 and
269 2.2 Ma, although this change is much more muted at DSDP 475 (Figure 4). We
270 also note that a recently-published record from Searles Lake does not cover this
271 entire interval, but does show a shift towards more positive δD_p values between
272 2.8 and 2.6 Ma, potentially in agreement with the pattern seen at CV (Peuple
273 et al., 2024). Both CV and Searles Lake also show similar reconstructed late
274 Pliocene δD_p values of between -80 and -70‰ , further increasing confidence in
275 our approach (Peuple et al., 2024).

276 **4. Discussion**

277 *4.1. Plio-Pleistocene ecosystem change in the southern Great Basin*

278 At an ecosystem scale, leaf wax carbon isotopes reflect changes in the relative
279 proportion of plants using the C₃ vs. C₄ photosynthetic pathways on the land-
280 scape. With this context, the trend towards more positive $\delta_{13}\text{C}$ values between
281 3 and 2 Ma in all three chain lengths of leaf wax n-acids likely reflects a small
282 increase in the representation of plants using the C₄ photosynthetic pathway in
283 the southern Great Basin. This could reflect an increase in the proportion of C₄
284 grasses on the landscape. However, recent work combining pollen and leaf wax
285 carbon isotopes found that in some regions of the arid southwest, a more C₄-like
286 signature can actually reflect a greater proportion of phreatophytic shrubs using
287 the C₄ photosynthetic pathway, like *Atriplex* (Peaple et al., 2024, 2022). The in-
288 crease in $\delta_{13}\text{C}$ values values in the CV record may therefore reflect long-term
289 shifts to either more C₄ grasses, or an increase in shrubs indicative of regional
290 shifts in water tables.

291

292 Other biomarker or pollen evidence would be needed to more clearly show the
293 type of vegetation shift that is responsible for the shift in leaf wax carbon isotopes.
294 However, we tentatively suggest that the long-term shift in carbon isotopes reflects
295 a greater proportion of C₄ grasses on the landscape as a result of greater aridity,
296 and a decrease in winter rainfall. Ecological literature from the Great Basin sug-
297 gests that reduced winter rainfall can favor the expansion of shallow-rooted plants
298 that include, but are not limited to, perennial C₄ grasses that facultatively use a

299 greater portion of summer moisture (Donovan and Ehleringer, 1994). In addi-
300 tion, C₄ photosynthesis tends to have a competitive advantage in warm, semi-arid
301 habitats (Sage et al., 1999). This conceptual model is supported by longer-term
302 Cenozoic records of habitat expansion, which found that C₄ grasslands expanded
303 with aridification in western-central North America (Kukla et al., 2022). Because
304 we have independent evidence of a progressive reduction in winter rainfall until
305 roughly from 2.8 to roughly 2.2 Ma (see section 4.2), we suggest that this likely
306 resulted in an expansion of C₄ grass habitats at the expense of woodland or shrub
307 environments in the southern Great Basin.

308 *4.2. Shifts in Rainfall Seasonality Between 2.6 and 2.2 Ma*

309 The CV leaf wax-inferred δD_p record shows an excursion to values near -60‰
310 between 2.6 and 2.2 Ma, after which time values of δD_p return to approximately
311 -95‰ . A similar excursion to more positive δD_p values is observed at ODP 1012,
312 though overall values of δD_p at this site are more enriched than at CV (Figure 4).
313 This likely reflects this site's proximity to the coast, while CV is located in the
314 lee side of the Sierra Nevada and the White Mountains, meaning that westerly air
315 masses that first begin to rain on the coast near site 1012 undergo significant vapor
316 distillation before reaching CV (Lechler and Galewsky, 2013; Mix et al., 2019).

317

318 We interpret a shift to more enriched δD_p values at CV as indicating a re-
319 duced contribution of winter rainfall relative to summer rainfall. In the desert
320 southwest, summer rainfall is more enriched in deuterium than winter rainfall

321 (Figure 1). This is likely because winter precipitation tends to have a greater pro-
322 portion of large-scale stratiform rainfall, compared to the summer, which tends to
323 feature more isotopically enriched deep convective rainfall (Aggarwal et al., 2016;
324 Schumacher and Funk, 2023). Other processes (e.g. large-scale shifts in mois-
325 ture source, sub-cloud re-evaporation, vapor recycling, and proximity to moisture
326 source) may also enhance the seasonal difference in precipitation isotopes (Eastoe
327 and Dettman, 2016; Bhattacharya et al., 2022). From this perspective, the posi-
328 tive excursion in δD_p values between 2.6 and 2.2 Ma could reflect a reduction in
329 winter rainfall to the CV region, resulting in a proportionally greater proportion
330 of summer rainfall. We note that a positive excursion between 2.6 and 2.2 Ma
331 also exists in $\delta^{18}D$ authigenic lacustrine carbonates from CV (see Gagnon et al.
332 (2023)). This shift in lacustrine carbonate isotopes could corroborate the reduc-
333 tion in winter moisture delivery and/or could reflect greater aridity, which would
334 result in greater evaporative demand from the lake basin.

335

336 Prior work has shown that summer rainfall in the southwest was higher in the
337 Pliocene, declining between 3.0 Ma and until roughly 2.25-2.5 Ma (Bhattacharya
338 et al., 2022). The interval between 2.6 and 2.2 Ma therefore likely had slightly
339 higher summertime rainfall than the late Pleistocene. We posit, however, that
340 the excursion between 2.6 and 2.2 Ma is not just the result of summer rainfall
341 changes, but also contains a signal related to a decrease in *independent* winter-
342 time precipitation, which would further amplify the proportional contribution of
343 summer rainfall to the annual rainfall budget. We next assess whether large-scale

344 climate conditions between 2.6 and 2.2 Ma are consistent with a decrease in winter
345 rainfall in this interval.

346 *4.3. Large-Scale Changes between 2.6 and 2.2 Ma*

347 Previous work, using a combination of models, observational data, and prox-
348 ies, suggests that long-term summertime precipitation changes in the southwest is
349 driven by the gradient of SST between the California margin and the eastern equa-
350 torial Pacific cold tongue (Bhattacharya et al., 2022, 2023). In contrast, other cli-
351 matic processes, especially at high latitudes, are critical drivers of the delivery of
352 winter rainfall by the midlatitude storm tracks. The position of the Aleutian Low
353 (AL) and the North Pacific Subtropical High (NPSH), semi-permanent centers of
354 low and high pressure respectively, modulate winter storm activity over western
355 North America (Giamalaki et al., 2021; Menemenlis et al., 2021). SST variabil-
356 ity in the equatorial Pacific, as well as extratropical modes of SST variability like
357 the Pacific Decadal Oscillation, influence the position, intensity, and frequency
358 of landfalling storms that impact western North America (Giamalaki et al., 2021;
359 Gan et al., 2017; Beaudin et al., 2023). From this perspective, large-scale changes
360 in SST patterns between 2.6 and 2.2 Ma could help bolster our argument about a
361 shift in rainfall seasonality between 2.6 and 2.0 Ma.

362

363 We note some evidence of warmer temperatures in the northeast Pacific be-
364 tween 2.6 and 2.0 Ma. An SST record from site U1417 in the Gulf of Alaska
365 shows an excursion to temperatures above 10°C between roughly 2.6 and 2.0

366 Ma (Sánchez-Montes et al., 2020) (Figure 5). In addition, an alkenone-based SST
367 record from Site 882, located in the western Bering Sea, shows a shift to slightly
368 warmer temperatures between 2.7 and 1.7 Ma (Yamamoto and Kobayashi, 2016)
369 (Figure 5). However, this high latitude warming does not likely reflect a canoni-
370 cal warm PDO-like pattern, which would involve warm SST anomalies extending
371 down the west coast of North America. Farther south, sites on the northern Cal-
372 ifornia Margin do not show an excursion to warmer temperatures in this time
373 period (LaRiviere et al., 2012; Brennan et al., 2022). Instead, sites like 1012,
374 1014, and 1010 show intensifying orbital-scale variability without any evidence
375 of a mean shift to warmer values between 2.0 and 2.6 Ma (Dekens et al., 2007;
376 Brierley et al., 2009). This suggests that warm SST anomalies in the Bering Sea
377 and Gulf of Alaska are not the result of a persistent warm PDO-like state. We also
378 note that there is no significant excursion in temperatures in the eastern equatorial
379 Pacific cold tongue between 2.0 and 2.6 Ma (Figure S2; Tierney et al. (2019)).
380 Therefore, the limited existing SST records suggest the presence of some high
381 latitude cooling in the north Pacific, relaxing the meridional temperature gradi-
382 ent over the northeastern Pacific, with impacts on rainfall anomalies over western
383 North America.

384

385 We compile a suite of SST records from across the north and equatorial Pacific
386 in order to assess whether latitudinal SST gradients weaken between 2.6 and 2.2
387 Ma (Liu et al., 2019; Seki et al., 2012; Rousselle et al., 2013; Shaari et al., 2013;
388 Etourneau et al., 2010; Herbert et al., 2016; Lawrence et al., 2006; LaRiviere et al.,

389 2012; Dekens et al., 2007; Brierley et al., 2009; Sánchez-Montes et al., 2020; Ya-
390 mamoto and Kobayashi, 2016; Brennan et al., 2022). All these records are based
391 on the alkenone paleothermometer, which uses the ratio of di- to tri- unsaturated
392 long-chain ketone compounds produced by haptophyte algae to quantitatively re-
393 construct SSTs (Herbert and Schuffert, 2000; Tierney and Tingley, 2018). We re-
394 calibrated each record using the latest Bayesian calibration (Tierney and Tingley,
395 2018), and interpolated values to a common 0.2 Ma timestep. We then took aver-
396 age SST anomalies between 2.8 and 2.6 Ma, prior to the positive excursion in our
397 leaf wax δD_p values, and between 2.3 and 2.4 Ma, within the interval where we
398 see a shift to more positive values in leaf wax δD_p . We also evaluate the strength
399 of this gradient between 1.5 and 1.7 Ma in order to see whether it steepens or
400 continues to relax following the excursion in δD_p (Figure S3).

401

402 We find that the interval between 2.3 and 2.4 Ma, when compared to the prior
403 (2.6-2.8 Ma) and subsequent (1.7 to 1.6 Ma) interval, exhibits a shallower gradient
404 of meridional gradient of temperature between 30 and 60° N. Between 2.8 and 2.6
405 Ma, we see that the north Pacific exhibits a meridional temperature gradient of
406 -0.58°C per ° latitude, similar to the slope seen between 1.6 and 1.7 Ma (-0.52°C
407 per ° latitude) (Figure 6, S3). However, between 2.3 and 2.4 Ma we find evidence
408 of a shallower meridional temperature gradient of -0.44°C per ° latitude, a change
409 that is significant at the 95% confidence interval (2-sided t-test) (Figure 6). This
410 shallower gradient is primarily driven by excursions to warmer temperatures at
411 sites like U1417 and ODP 882, coupled with strong cooling at subtropical sites

412 like 1012 and 1014.

413

414 We note that this shift in the latitudinal gradient is constrained by relatively
415 few sites at high northern latitudes, and that prior work suggests that several sites
416 may primarily reflect summer or fall SSTs, rather than an annually averaged sig-
417 nal. However, some sediment trap work near site 882 suggests that alkenone-
418 based SSTs at this site may represent late fall (November) temperatures (Sánchez-
419 Montes et al., 2020; Yamamoto and Kobayashi, 2016; Harada et al., 2006). De-
420 spite the uncertainties associated with the sparse north Pacific SST record, our
421 results suggest that the meridional temperature gradient over the Pacific is shal-
422 lower during start of the Pleistocene (e.g. 2.6 to 2.0 Ma) compared to late Pliocene
423 (3.0 to 2.7 Ma). This runs counter to the general assumption that the meridional
424 SST gradient should steepen in response to global cooling and glacial intensifi-
425 cation over the Plio-Pleistocene transition. While the causes of this shift remain
426 mysterious and are outside the scope of the current work, it is possible that they
427 are related to shifts in deep ocean circulation in the Pacific (Burls et al., 2017).
428 We next explore the potential consequences of this shift for regional hydroclimate
429 in western North America.

430 *4.4. Dynamical Mechanisms*

431 Between 2.6 and 2.0 Ma, warm SSTs in the high-latitude Pacific likely re-
432 duced the intensity of winter storms hitting the central-west coast of North Amer-
433 ica. Modern observations suggest that cool SST anomalies in the Gulf of Alaska

434 and Bering Sea in late summer and early fall often persist into winter and help
435 enhance winter storm tracks to the north of 30°N. This is because cool high lat-
436 itude SSTs amplify the meridional gradient of temperature, increasing baroclin-
437 icity and cyclogenesis over the northeast Pacific (Pickart et al., 2009; Gan and
438 Wu, 2013). Idealized model simulations show that a steeper meridional SST gra-
439 dient over the north Pacific increases transient eddy activity and strengthens the
440 polar (eddy-driven) jet (Wang et al., 2019). From this perspective, the warming
441 of the Bering Sea and Gulf of Alaska would reduce baroclinicity and storm activ-
442 ity, reducing the winter storms in southwestern North America. This reduction in
443 winter rainfall would likely also influence ODP 1012, which is located near 30°N,
444 but would likely not have a major influence on DSDP 475, which is farther south
445 (Figure 3). This could explain the shift to more enriched δD_p values, indicative of
446 a reduction in winter storm activity, most prominently at CV and ODP 1012. High
447 latitude temperatures may also influence summer rainfall, but prior work suggests
448 that subtropical temperatures are more important in governing monsoon strength
449 (Bhattacharya et al., 2022, 2023).

450

451 To further explore the dynamical linkage between north Pacific temperatures
452 and hydroclimate in the region around CV, we analyze two simulations of the
453 isotope-enabled version of the Community Earth System Model, version 1.2 (iCESM1.2).
454 These model simulations, described in detail in Bhattacharya et al. (2022), are run
455 with fixed SST fields in atmosphere-only mode (e.g. with the Community At-
456 mospheric Model version 5, or iCAM5), at an $0.9^\circ \times 1.25^\circ$ horizontal resolution,

457 with 30 vertical layers. While relatively low resolution, this model configuration
458 captures the observed seasonal cycle of precipitation isotopes in the southwest
459 (Bhattacharya et al., 2022). SSTs are taken from a pre-industrial control simula-
460 tion for the ‘control’ experiment, while for the experimental run, SSTs are taken
461 from the SST pattern from a mid-to-late Pliocene simulation of CESM2 presented
462 in Feng et al. (2020), with 2° of uniform added on top of this SST pattern. We
463 refer to this as the ‘relaxed gradient experiment’ This simulation produces pole-
464 ward amplified warming over the North Pacific, with the strongest temperature
465 anomalies in the Bering Sea, northwest Pacific, and Gulf of Alaska (Figure 7).
466 There is also a small warming of the cold tongue in the eastern equatorial Pa-
467 cific. This simulation should therefore not be taken as a realistic simulation of
468 the late Pliocene/early Pleistocene, but rather as a sensitivity experiment to an-
469 alyze the response of regional hydroclimates to large-scale SST gradients. The
470 pattern of SST change in the experimental simulation is different than the SST
471 anomalies we think occurred between 2.6 and 2.0 Ma, which we show primarily
472 involved poleward amplified warming and a relaxed latitudinal gradient, without a
473 distinct shift in equatorial Pacific temperatures (Figure S2). Nonetheless, our ex-
474 perimental simulation is still useful for exploring how regional hydroclimate shifts
475 in response to a relaxed latitudinal temperature gradient, helping us investigate the
476 hypothesis that latitudinal gradients helped drive rainfall changes between 2.6 and
477 2.0 Ma.

478

479 Compared to the pre-industrial control, our relaxed gradient experiment pro-

480 duces wintertime drying over southwestern North America and wetter conditions
481 poleward over 40°N. This is accompanied by an anomalous cyclonic circulation
482 in the northeast Pacific, as well as a weakening of westerly winds near 60°N as
483 well as equatorward of the low pressure center, near 25°N. While the low pressure
484 could result from teleconnection patterns triggered by warming of the equatorial
485 Pacific cold tongue, the rainfall pattern in Figure 7 does not resemble a canonical
486 ENSO teleconnection pattern, which would predict wetter conditions in southwest
487 North America in the wintertime (Goldner et al., 2011). We suggest that the pole-
488 ward shift in rainfall results from a poleward shift of storm tracks in response to
489 a relaxed latitudinal gradient. This in turn drives decreased cool season rainfall in
490 the region around Clayton Valley, which sits on the edge of the region experienc-
491 ing drying in this relatively low-resolution model simulation. A spatial average of
492 rainfall anomalies in the region around Clayton Valley (30 to 38°N and 120 to 100
493 W) shows that the region indeed experiences a decrease in cool season rainfall,
494 especially in October and November as well as in February-April, and a slight
495 increase in summer rainfall. This is consistent with our conceptual explanation of
496 the CV leaf wax record in section 4.2.

497

498 In the relaxed gradient experiment, precipitation isotopes are heavier in all
499 months relative to pre-industrial (Figure 7c), likely as a result of warmer tempera-
500 tures in the experimental simulation. These results are broadly consistent with our
501 interpretation of the shift to more positive δD_p between 2.6 and 2.0 Ma: a decrease
502 in the relative proportion of winter rainfall, which tends to be more isotopically

503 depleted, and an increase in summer rainfall, which is typically more enriched in
504 deuterium, would result in a shift to more enriched δD_p values. This would be
505 further enhanced by an overall shift to more enriched δD_p values in all months
506 of the year. While isotope-enabled models do not capture all the microphysical
507 processes that influence precipitation isotopes (e.g. distinct signatures of convec-
508 tive versus stratiform rainfall) (Hu et al., 2018), the results of this simulation are
509 broadly consistent with our dynamical interpretation of the Clayton Valley record.
510 Given this simulation, and our independent proxy evidence of a relaxed latitudinal
511 gradient of temperature between 2.6 and 2.0 Ma, we suggest that this time period
512 was characterized by a decrease in winter storms in southwestern North America,
513 largely as the result of a poleward shift of the jet driven by a shallower merid-
514 ional temperature gradient. This decrease in winter rainfall was superimposed on
515 a long-term trend towards decreasing summer rainfall over the Plio-Pleistocene
516 transition (Bhattacharya et al., 2022).

517 *4.5. Implications for Li Resources*

518 The CV Plio-Pleistocene stable isotope records, from both carbonates and leaf
519 waxes, suggests that the interval between 2.6 and 2.0 Ma was a time of hydrocli-
520 matic reorganization, within a broader climatic transition over the Pliocene to the
521 Pleistocene. This involved a shift from a larger contribution of summer rainfall in
522 the Pliocene, punctuated by a reduced contribution of winter rainfall between 2.6
523 and 2.0 Ma, as inferred from our proxy records and supported by model simula-
524 tions. A comparison to bulk sedimentological properties suggests that the maxi-

525 mum concentrations of sedimentary lithium occur at roughly 2.6-2.5 Ma, and that
526 there is a slow downward trend in lithium accumulations in sediments after 2.0 Ma
527 (Figure 8). Here, we infer a process-based link based on the long term trends and
528 short term variations from EXP2's carbonate and leaf wax stable isotope records,
529 lithology, and whole rock lithium dataset.

530

531 First, the leaf wax δD_p record indicates a decrease of at least 20‰ to as much
532 as 50‰ from $\tilde{2.6}$ Ma to present. Similarly, after an initial increase from 2.9 to 2.6
533 Ma, the least evaporatively enriched $\delta^{18}O_{carb}$ values across the carbonate stable
534 isotope timeseries decline approximately 7‰ from 2.6 Ma to present ((Figure 8).
535 Assuming scaling similar to the global meteoric water line (e.g. 1:8 ratio of $\delta^{18}O$
536 to δD), a 7‰ decline in $\delta^{18}O$ is greater than would be inferred from a 20‰ de-
537 crease in δD_p . However, it would be a majority of the signal inferred from a 50‰
538 decrease in δD_p . As such, this confirms previous interpretations that the light-
539 est $\delta^{18}O_{carb}$ values represented relatively unevaporated meteoric waters (Gagnon
540 et al., 2023) and the periods of the greatest $\delta^{18}O_{carb}$ was likely caused by enhanced
541 evaporation.

542

543 Second, our new measurements of lithium concentrations and carbonate stable
544 isotope data suggest that the period of greatest lithium accumulation occurs dur-
545 ing a time period of hydroclimate transition and high evaporation, near 2.6 Ma.
546 Enriched $\delta^{18}O_{carb}$ values and lithium concentrations are observed in both the bulk
547 sediments (Gagnon et al., 2023) and modern brines (Coffey et al., 2021). Across

548 the record evapoconcentration of lake water appears to drive both carbonate oxy-
549 gen isotopes towards higher values (due to the preferential evaporation of oxygen-
550 16) and concentrate lithium in the paleolake in Clayton Valley. Even including our
551 new data, the correlation between $\delta^{18}\text{O}_{carb}$ and Li concentrations remains strong
552 ($r=0.54$), similar to the correlations in Gagnon et al. (2023). During the period
553 of inferred hydroclimate reorganization based on the new leaf wax datasets, bulk
554 lithium concentrations are between 500 and 2,000 ppm (upper continental crust
555 is 35 ppm; Teng et al. (2004)) and are at their highest sustained values between
556 2.3 and 2.6 Ma.

557

558 Shifts in hydroclimate seasonality, as inferred from leaf wax δD_p data and our
559 proxy-model comparison, would enhance lithium accumulations in the Clayton
560 Valley paleolake. Intense summertime convective storms falling in warm condi-
561 tions during the late Pliocene would favor increased weathering of the surrounding
562 catchments driving enhanced lithium delivery to the paleolake in Clayton Valley.
563 Warm season, intense rainfall would likely drive stronger weathering than cool
564 season precipitation. Reduced winter rainfall (e.g. at 2.6 Ma) would enhance win-
565 tertime evaporative demand from the lake, pushing carbonate oxygen isotopic
566 values to heavier values and increasing solute concentrations in the paleolake and
567 regional soil and groundwater. These processes would enhance lithium transport
568 to and evapoconcentration in the paleolake. Furthermore, hot spring contributions
569 (Coffey et al., 2021) to the lake could have also been enhanced via increased in-
570 teraction of meteoric waters delivered during intense summer storms with range

571 bounding faults. These processes would likely culminate in the highest concen-
572 trations of lithium, as well as the most enriched $\delta^{18}\text{O}_{carb}$ values, between roughly
573 2.6 and 2.5 Ma. Subsequent to 2.0 Ma, with reductions in summer rainfall and
574 long-term shifts to a winter-dominated signal, despite largely similar facies (la-
575 custrine clays) until approximately 0.7 Ma, less lithium was delivered to the lake
576 basin resulting in lower bulk lithium values.

577

578 Given these observations linking the carbonate and leaf wax stable isotope
579 records to lithium accumulation in the EXP2 core, we contend that rainfall sea-
580 sonality driving weathering reactions on the landscape likely played an important
581 role, in addition to evapoconcentration of the paleolake, in lithium enrichment in
582 Clayton Valley. Such a process-based link is likely to be found in other closed
583 basins with lithium rich clay deposits.

584

585 **5. Conclusions**

586 In this paper, we presented a new Plio-Pleistocene record of leaf wax carbon
587 and hydrogen isotopes from Clayton Valley, Nevada. This record, which spans
588 the interval from approximately 2.8 Ma to the present, provides an unprecedented
589 view of changes in the seasonality of rainfall from the Great Basin. Analyses of 3
590 different chain lengths of leaf waxes show a shift to more enriched values between
591 roughly 2.6 and 2.0 Ma, at the start of the Quaternary and coincident with global
592 cooling and the inception of northern hemisphere glaciation. This interval is also

593 characterized by more positive values of $\delta^{18}\text{O}$ of authigenic carbonate, and an
594 increase in lithium concentrations in sediments. Other regional leaf wax records
595 also include an excursion to more positive δD_p values in this interval. We interpret
596 this positive shift as a northward shift or a decrease in the intensity of winter storm
597 tracks, resulting in summer rainfall providing a greater share of annual rainfall.
598 This pattern is super-imposed on a long-term decline in summertime rainfall from
599 3.0 to roughly 2.0-2.5 Ma.

600

601 Warming in the high latitude Pacific Ocean likely contributed to the reduction
602 in winter rainfall at the start of the Pleistocene. In modern observational data, cool
603 SST anomalies in the Gulf of Alaska and Bering Sea is linked to an increase in
604 winter storm activity over western North America, while anomalously warm tem-
605 peratures reduce transient eddy activity. While only a few continuous SST records
606 are available from the Plio-Pleistocene high northern latitude Pacific, available
607 data does suggest a relaxation of the latitudinal temperature gradient between 2.6
608 and 2.0 Ma. This would support a reduction in North Pacific storm activity within
609 this interval, though more data is needed to precisely constrain SST gradients.
610 There is no evidence of a shift in the equatorial Pacific SST gradient at this time.
611 We find support for this view in a simulation of the isotope-enabled Community
612 Atmospheric Model (iCAM5) which, when forced with a relaxed meridional tem-
613 perature gradient in the Pacific, results in a northward shift in wintertime storm
614 activity and a drying of the region near Clayton Valley and ODP 1012. In this
615 simulation, δD_p becomes more enriched, partially as a result of an increase in en-

616 riched summer rainfall and a decrease in depleted winter rainfall. There is also an
617 increase in the isotopic signature of rainfall in all months, likely as a result of over-
618 all warmer temperatures in the uniform warming compared to the pre-industrial
619 simulation.

620

621 It is possible that non-climatic factors exerted an influence on the Clayton
622 Valley record. First, Quaternary orographic changes (e.g. uplift of the White
623 Mountains and the Sierra Nevada) could result in a change in moisture trajecto-
624 ries, or the degree of orographic rainout of winter storms, upstream from Clayton
625 Valley. This would likely result in a long-term depletion trend in the CV record,
626 but would not necessarily influence coastal records like ODP 1012. However, oro-
627 graphic rainout is unlikely to result in a distinct, temporally constrained *increase*
628 in δD_p between 2.6 and 2.0 Ma, and the fact that we see this shift at both CV and
629 ODP 1012 also adds confidence to our interpretation. With respect to lithium, it is
630 possible that local tectonics exposed lithium-rich source rocks at roughly 2.6 Ma,
631 enhancing lithium delivery via enhanced weathering of the basin's watersheds.
632 While this remains possible, after 2.9 Ma the only major lithologic change in sed-
633 iments occurs at approximately 800 ka (Gagnon et al., 2023), as sedimentation
634 from the basin's alluvial fans increasingly encroach on the EXP 2 core location.
635 From 800 ka to present, dilution due to coarser grain sized alluvial fan sediments
636 may be the source of whole rock lithium concentrations decreasing. Further sed-
637 imentological and geochemical analyses from depocenter cores (to the northwest
638 of EXP 2), and on clay separates, would be necessary to test the possibility of

639 local tectonics influencing lithium delivery to the basin's lacustrine sediments.
640 However, as the large-scale lithium concentration trends in EXP 2 are mirrored in
641 two other deep cores covering the same time interval from the southern sub-basin
642 of CV (Coffey et al., 2021) we propose that the CV sediments record a wholesale
643 response to hydroclimate in the lithium concentration trends observed with depth.

644

645 Overall, our results suggest that the Plio-Pleistocene transition involved a sig-
646 nificant reorganization of rainfall regimes in southwestern North America. While
647 previous studies have shown that the Pliocene was characterized by a greater pro-
648 portion of summer rainfall, the record from CV, along with our SST compila-
649 tion and model simulation, suggest that, instead of a steady long-term trend to a
650 greater dominance of winter rainfall in the southern Great Basin, the late Pliocene
651 and early Pleistocene featured a punctuated climatic interval between 2.0 and 2.6
652 Ma with reduced winter rainfall. This underscores the sensitivity of rainfall in
653 western North America to large-scale SST gradients. Further work to constrain
654 the dynamics of winter rainfall changes over the Plio-Pleistocene could provide
655 constraints on the sensitivity of precipitation regimes in western North America
656 to large-scale shifts in past and future SST patterns.

657

658 Finally, it is notable that the interval between 2.6 and 2.0 Ma coincides with a
659 time period of greater enrichment of lithium in the CV lake sediments, highlight-
660 ing the long-term coupling of hydroclimatic regime changes and the formation
661 of economically important lithium-rich brines and claystones in the desert south-

662 west. Our combined interpretation of existing inorganic geochemical proxies and
663 our organic proxies suggests that it was not just aridity that exerted an important
664 influence on the development of lithium resources in the southwest, but rather
665 a shift in the seasonality of the rainfall regimes. Our work therefore highlights
666 the long-term coupling between precipitation seasonality, and hydroclimate more
667 generally, with the formation of economically important deposits of a key 21st
668 century critical mineral.

669 **6. Acknowledgments**

670 TB acknowledges funding from NSF P2C2 Grant OCE-1903148 and NSF
671 CAREER Award OCE-2237502. DEI acknowledges funding from NSF P2C2
672 grant AGS-2102901 and the Institute at Brown for Environment and Society. We
673 thank Bryce Belanger (Vanderbilt) and Matthew Bolton (University of Alberta)
674 for field assistance and help identifying ash layers in cores from CV. Andrew
675 Cooper (Thermo) and Christopher Maupin (Texas A&M) provided essential in-
676 strumentation support. We thank Albemarle Corporation for providing logistical
677 support and access to cores. Data will be permanently archived in the NOAA
678 Paleoclimatology Database upon acceptance of this manuscript.

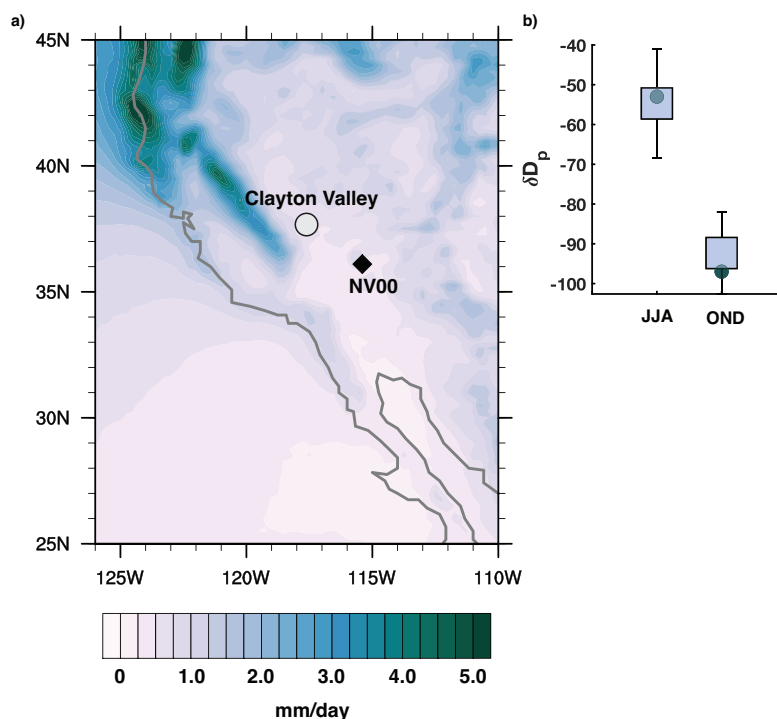


Figure 1: **Study region and background climatology.** a) Background colors indicate annual average rainfall rates over western US, with the location of Clayton Valley (CV) and the isotope monitoring site (NV-00) indicated on the map. b) shows amount-weighted estimate of δD of precipitation in summer (JJA) and winter (OND) from NV-00 in boxplots with $1-\sigma$ error bars, with circles indicating estimated seasonal precipitation isotopic composition from the Online Isotopes in Precipitation Calculator (Bowen and Revenaugh, 2003). Seasonal intervals chosen to maximize the data availability at the NV-00 data (e.g. very little data from September was available).

679 **References**

- 680 Aggarwal, P.K., Romatschke, U., Araguas-Araguas, L., Belachew, D., Longstaffe,
 681 F.J., Berg, P., Schumacher, C., Funk, A., 2016. Proportions of convective and
 682 stratiform precipitation revealed in water isotope ratios. *Nature Geoscience* 9,
 683 624–629.
- 684 Almazroui, M., Islam, M.N., Saeed, F., Saeed, S., Ismail, M., Ehsan, M.A.,

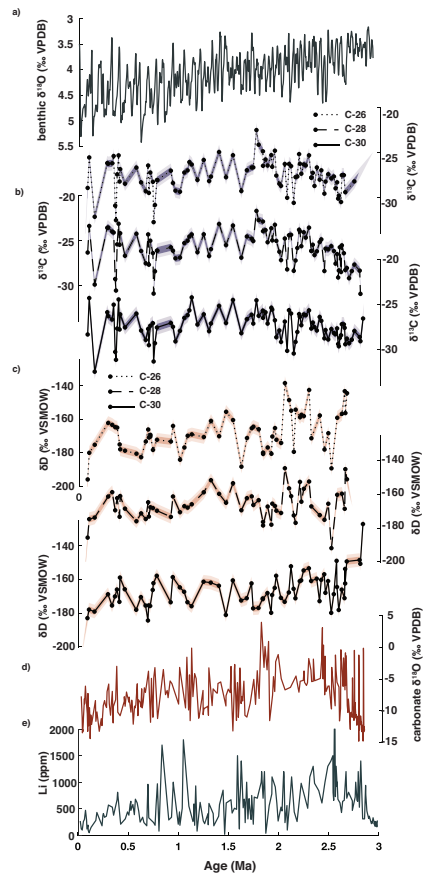


Figure 2: **Raw isotopic data from Clayton Valley.** a) shows the benthic oxygen isotope stack from Westerhold et al. (2020) for context. Panel b) shows carbon isotopic data from three long-chain leaf waxes (e.g. the C-26, C-28, and C-30) alkanolic acid); while c) shows hydrogen isotopic data from the same leaf wax chain lengths. d) shows previously published oxygen isotope data from authigenic lacustrine carbonates from Gagnon et al. (2023), supplemented with additional data, while e) shows Li concentration data from the Clayton Valley core, from Gagnon et al. (2023) and Coffey et al. (2021), with some new data reported in this study

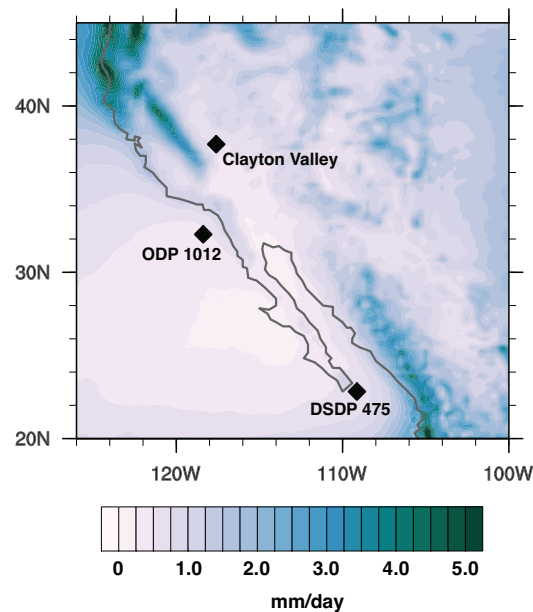


Figure 3: **Location of Plio-Pleistocene δD of precipitation reconstructions.** Clayton Valley data is from this study, while ODP 1012 and DSDP 475 were published in Bhattacharya et al. (2022).

685 Diallo, I., O'Brien, E., Ashfaq, M., Martínez-Castro, D., Cavazos, T.,
 686 Cerezo-Mota, R., Tippett, M.K., Gutowski, W.J., Alfaro, E.J., Hidalgo, H.G.,
 687 Vichot-Llano, A., Campbell, J.D., Kamil, S., Rashid, I.U., Sylla, M.B.,
 688 Stephenson, T., Taylor, M., Barlow, M., 2021. Projected Changes in Tem-
 689 perature and Precipitation Over the United States, Central America, and the
 690 Caribbean in CMIP6 GCMs. *Earth Systems and Environment* 5, 1–24. URL:
 691 <http://link.springer.com/10.1007/s41748-021-00199-5>,
 692 doi:10.1007/s41748-021-00199-5.

693 Beaudin, É., Di Lorenzo, E., Miller, A., Seo, H., Joh, Y., 2023. Impact of Extra-
 694 tropical Northeast Pacific SST on US West Coast Precipitation. *Geophysical*
 695 *Research Letters* 50, e2022GL102354.

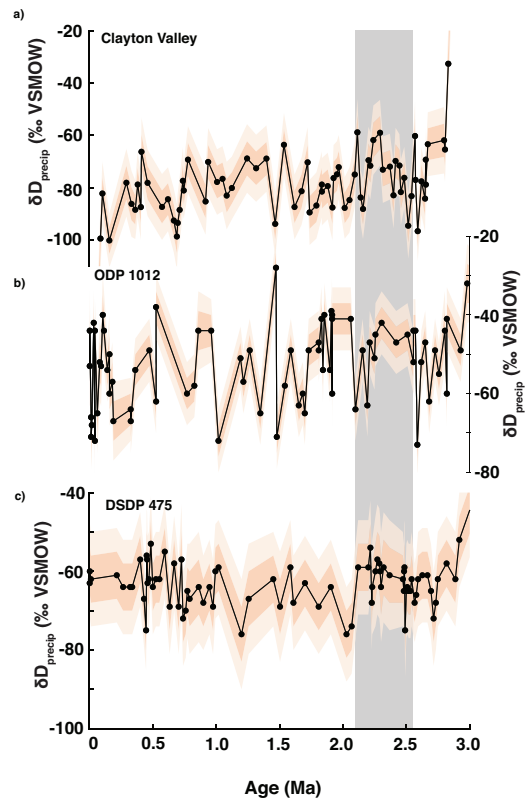


Figure 4: Leaf wax δD of precipitation reconstructions from southwestern North America. a) shows Clayton Valley record, presented in this paper; b) and c) show the records from ODP 1012 and DSDP 475, presented in (Bhattacharya et al., 2022). All records are based on the C_{30} n-acid.

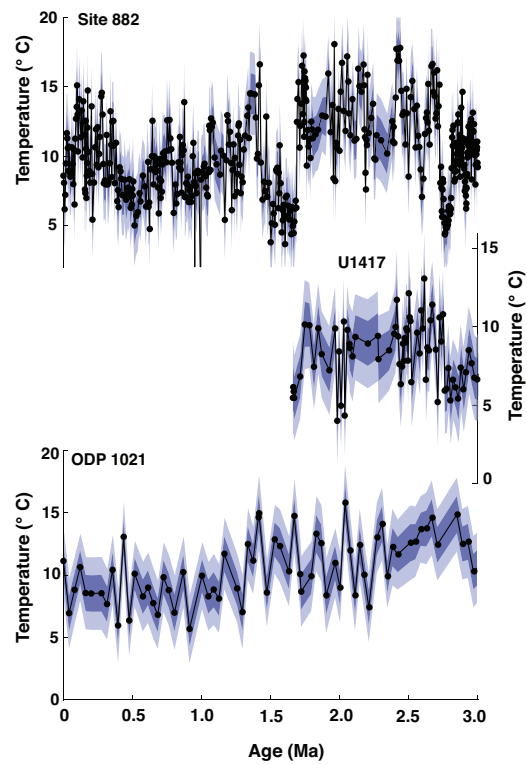


Figure 5: **East Pacific extratropical SST records covering the interval from 3.0 Ma to present.** a) shows the record from the western Bering Sea from Site 882 (Yamamoto and Kobayashi, 2016); b) shows the record from U1417 in the Gulf of Alaska (Sánchez-Montes et al., 2020)l while c) shows Site 1021 on the northern California Margin (LaRiviere et al., 2012)

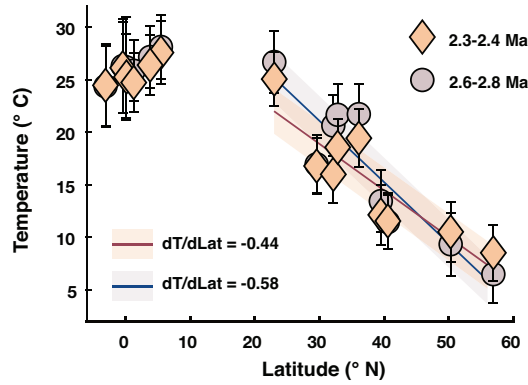


Figure 6: **Pacific Latitudinal SST Gradients prior to and during early Pleistocene.** Comparing and contrasting the extratropical meridional temperature gradient between 2.6 and 2.8 Ma (blue circles) and 2.3 and 2.4 Ma (orange triangles) over the Pacific Ocean. A least-squares regression line is calculated between 20 and 60 ° N to emphasize the difference in slope between these two intervals. See Supplementary Figure 3 for SST gradients at 1.7 Ma, and text for more details on the SST proxy compilation.

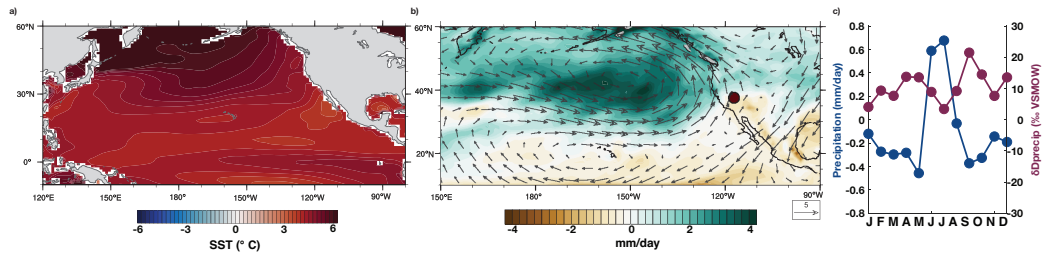


Figure 7: **Atmospheric Changes in iCAM5 in PI Control compared to 2x Uniform Warming.** a) SST difference between 2x uniform warming simulation and PI ($1xCO_2$) simulation. SST patterns are prescribed in both simulations, and are taken from a fully coupled simulation (see Bhattacharya et al. (2022)) b) Winter (DJF) precipitation as well as 850 mb wind differences in these simulations; c) Anomalies of monthly precipitation (blue) and δD_p (maroon)

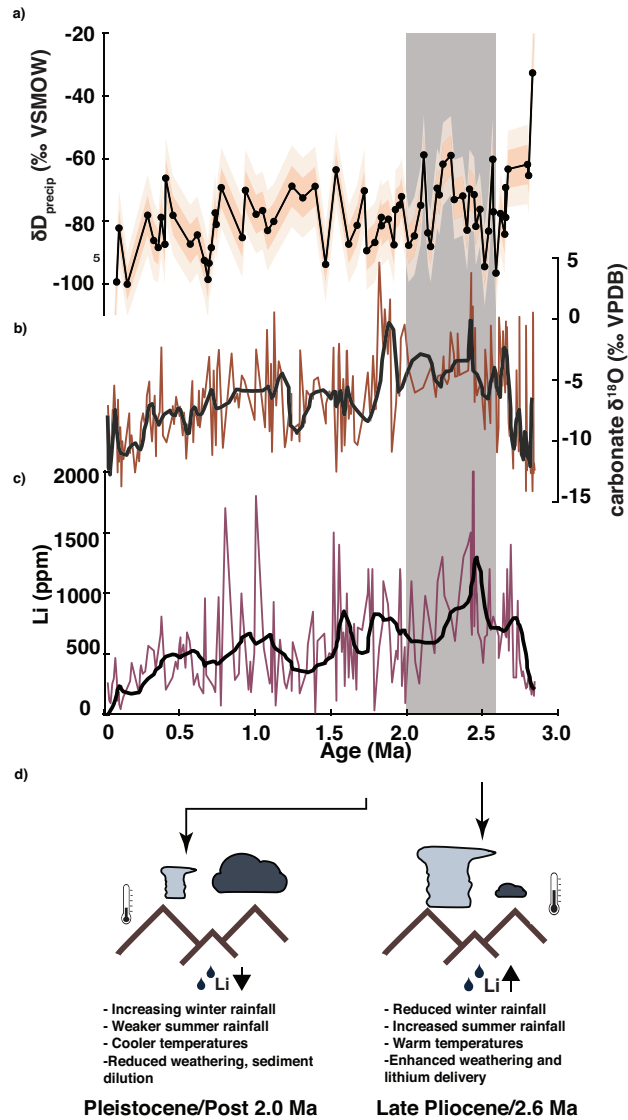


Figure 8: **Summary of environmental changes at CV and relationship to lithium enrichment.** a) δD_p reconstruction from Clayton Valley; b) authigenic carbonate oxygen isotope data and c) bulk sediment lithium concentration in ppm (oxygen isotope data and lithium concentrations are previously shown in Figure 2). d) summary cartoon of climate changes in late Pliocene (roughly 2.6 Ma) and the Pleistocene during the interval after 2.0 Ma.

- 696 Benson, T.R., Coble, M.A., Dilles, J.H., 2023. Hydrothermal enrichment of
697 lithium in intracaldera illite-bearing claystones. *Science Advances* 9, eadh8183.
- 698 Bhattacharya, T., Feng, R., Maupin, C.R., Coats, S., Brennan, P.R.,
699 Carter, E., 2023. California margin temperatures modulate re-
700 gional circulation and extreme summer precipitation in the desert
701 Southwest. *Environmental Research Letters* 18, 104048. URL:
702 <https://iopscience.iop.org/article/10.1088/1748-9326/acfd43>,
703 doi:10.1088/1748-9326/acfd43.
- 704 Bhattacharya, T., Feng, R., Tierney, J.E., Rubbelke, C., Burls, N., Knapp, S.,
705 Fu, M., 2022. Expansion and intensification of the North American Monsoon
706 during the Pliocene. *AGU Advances* 3, e2022AV000757.
- 707 Bhattacharya, T., Tierney, J.E., Addison, J.A., Murray, J.W., 2018. Ice-sheet
708 modulation of deglacial North American monsoon intensification. *Nature Geo-
709 science* 11, 848–852.
- 710 Blaauw, M., Christen, J.A., Bennett, K., Reimer, P.J., 2018. Double the dates
711 and go for Bayes—Impacts of model choice, dating density and quality on
712 chronologies. *Quaternary Science Reviews* 188, 58–66.
- 713 Bowen, G.J., Revenaugh, J., 2003. Interpolating the isotopic composition of mod-
714 ern meteoric precipitation. *Water resources research* 39.
- 715 Brennan, P.R., Bhattacharya, T., Feng, R., Tierney, J.E., Jorgensen, E.M.,
716 2022. Patterns and mechanisms of northeast Pacific temperature response to

717 Pliocene boundary conditions. *Paleoceanography and Paleoclimatology* 37,
718 e2021PA004370.

719 Brierley, C.M., Fedorov, A.V., Liu, Z., Herbert, T.D., Lawrence, K.T., LaRiviere,
720 J.P., 2009. Greatly expanded tropical warm pool and weakened Hadley circu-
721 lation in the early Pliocene. *Science* 323, 1714–1718.

722 Burls, N.J., Fedorov, A.V., Sigman, D.M., Jaccard, S.L., Tiedemann, R., Haug,
723 G.H., 2017. Active Pacific meridional overturning circulation (PMOC) during
724 the warm Pliocene. *Science Advances* 3, e1700156.

725 Choi, J., Lu, J., Son, S., Frierson, D.M.W., Yoon, J., 2016. Un-
726 certainty in future projections of the North Pacific subtropical high
727 and its implication for California winter precipitation change. *Jour-
728 nal of Geophysical Research: Atmospheres* 121, 795–806. URL:
729 <https://onlinelibrary.wiley.com/doi/10.1002/2015JD023858>,
730 doi:10.1002/2015JD023858.

731 Coffey, D., Munk, L.A., Ibarra, D., Butler, K., Boutt, D., Jenckes, J., 2021.
732 Lithium storage and release from lacustrine sediments: Implications for lithium
733 enrichment and sustainability in continental brines. *Geochemistry, Geophysics,
734 Geosystems* 22, e2021GC009916.

735 Collister, J.W., Rieley, G., Stern, B., Eglinton, G., Fry, B., 1994. Compound-
736 specific $\delta^{13}\text{C}$ analyses of leaf lipids from plants with differing carbon dioxide
737 metabolisms. *Organic geochemistry* 21, 619–627.

- 738 Cook, B.I., Seager, R., 2013. The response of the North American
739 Monsoon to increased greenhouse gas forcing: NA MONSOON AND
740 GHG WARMING. *Journal of Geophysical Research: Atmospheres* 118,
741 1690–1699. URL: <http://doi.wiley.com/10.1002/jgrd.50111>,
742 doi:10.1002/jgrd.50111.
- 743 Davis, J.R., Friedman, I., Gleason, J., 1986. Origin of the lithium-rich brine,
744 clayton valley, nevada. *US Geological Survey Bulletin* 1622, 131–138.
- 745 Dekens, P.S., Ravelo, A.C., McCarthy, M.D., 2007. Warm upwelling regions in
746 the pliocene warm period. *Paleoceanography* 22.
- 747 Donovan, L., Ehleringer, J., 1994. Water stress and use of summer precipitation
748 in a Great Basin shrub community. *Functional Ecology* , 289–297.
- 749 Eastoe, C., Dettman, D., 2016. Isotope amount effects in hydrologic and climate
750 reconstructions of monsoon climates: Implications of some long-term data sets
751 for precipitation. *Chemical Geology* 430, 78–89.
- 752 Etourneau, J., Schneider, R., Blanz, T., Martinez, P., 2010. Intensification of the
753 Walker and Hadley atmospheric circulations during the Pliocene–Pleistocene
754 climate transition. *Earth and Planetary Science Letters* 297, 103–110. URL:
755 <https://www.sciencedirect.com/science/article/pii/S0012821X10003845>,
756 doi:10.1016/j.epsl.2010.06.010.
- 757 Feng, R., Otto-Bliesner, B.L., Brady, E.C., Rosenbloom, N., 2020. Increased cli-
758 mate response and Earth system sensitivity from CCSM4 to CESM2 in mid-

759 Pliocene simulations. *Journal of Advances in Modeling Earth Systems* 12,
760 e2019MS002033.

761 Gagnon, C.A., Butler, K.L., Gaviria, E., Terrazas, A., Gao, A., Bhattacharya, T.,
762 Boutt, D.F., Munk, L.A., Ibarra, D.E., 2023. Paleoclimate controls on lithium
763 enrichment in Great Basin Pliocene- Pleistocene lacustrine clays. *Geological*
764 *Society of America Bulletin* .

765 Gan, B., Wu, L., 2013. Seasonal and Long-Term Coupling be-
766 tween Wintertime Storm Tracks and Sea Surface Temperature in
767 the North Pacific. *Journal of Climate* 26, 6123–6136. URL:
768 <http://journals.ametsoc.org/doi/10.1175/JCLI-D-12-00724.1>,
769 doi:10.1175/JCLI-D-12-00724.1.

770 Gan, B., Wu, L., Jia, F., Li, S., Cai, W., Nakamura, H., Alexander, M.A., Miller,
771 A.J., 2017. On the response of the Aleutian low to greenhouse warming. *Journal*
772 *of Climate* 30, 3907–3925.

773 Gao, L., Edwards, E.J., Zeng, Y., Huang, Y., 2014. Major evolutionary trends
774 in hydrogen isotope fractionation of vascular plant leaf waxes. *PloS one* 9,
775 e112610.

776 Giamalaki, K., Beaulieu, C., Henson, S.A., Martin, A.P., Kassem, H.,
777 Faranda, D., 2021. Future intensification of extreme Aleutian low
778 events and their climate impacts. *Scientific Reports* 11, 18395. URL:

779 <https://www.nature.com/articles/s41598-021-97615-7>,
780 doi:10.1038/s41598-021-97615-7.

781 Goldner, A., Huber, M., Diffenbaugh, N., Caballero, R., 2011. Implications of
782 the permanent El Niño teleconnection’ blueprint’ for past global and North
783 American hydroclimatology. *Climate of the Past* 7, 723–743.

784 Harada, N., Sato, M., Shiraishi, A., Honda, M.C., 2006. Characteristics of
785 alkenone distributions in suspended and sinking particles in the northwestern
786 North Pacific. *Geochimica et Cosmochimica Acta* 70, 2045–2062.

787 Herbert, T.D., Lawrence, K.T., Tzanova, A., Peterson, L.C., Caballero-
788 Gill, R., Kelly, C.S., 2016. Late Miocene global cooling and
789 the rise of modern ecosystems. *Nature Geoscience* 9, 843–847.
790 URL: <https://www.nature.com/articles/ngeo2813>,
791 doi:10.1038/ngeo2813. number: 11 Publisher: Nature Publishing Group.

792 Herbert, T.D., Schuffert, J.D., 2000. 16. alkenone unsaturation estimates of sea-
793 surface temperatures at site 1002 over a full glacial cycle, in: *Proceedings of*
794 *the Ocean Drilling Program, Scientific Results*, pp. 239–247.

795 Hu, J., Emile-Geay, J., Nusbaumer, J., Noone, D., 2018. Impact of Convective
796 Activity on Precipitation δ 18O in Isotope-Enabled General Circulation Models.
797 *Journal of Geophysical Research: Atmospheres* 123, 13–595.

798 Ibarra, D.E., Oster, J.L., Winnick, M.J., Caves Rügenstein, J.K., Byrne, M.P.,

799 Chamberlain, C.P., 2018. Warm and cold wet states in the western United
800 States during the Pliocene–Pleistocene. *Geology* 46, 355–358.

801 Inglis, G.N., Bhattacharya, T., Hemingway, J.D., Hollingsworth, E.H., Feakins,
802 S.J., Tierney, J.E., 2022. Biomarker approaches for reconstructing terrestrial
803 environmental change. *Annual Review of Earth and Planetary Sciences* 50,
804 369–394.

805 King, K.E., Cook, E.R., Anchukaitis, K.J., Cook, B.I., Smerdon, J.E., Seager,
806 R., Harley, G.L., Spei, B., 2024. Increasing prevalence of hot drought across
807 western North America since the 16th century. *Science Advances* 10, eadj4289.

808 Kukla, T., Rugenstein, J., Ibarra, D.E., Winnick, M., Strömberg, C.A., Chamber-
809 lain, C., 2022. Drier winters drove Cenozoic open habitat expansion in North
810 America. *AGU Advances* 3, e2021AV000566.

811 LaRiviere, J.P., Ravelo, A.C., Crimmins, A., Dekens, P.S., Ford, H.L., Lyle, M.,
812 Wara, M.W., 2012. Late Miocene decoupling of oceanic warmth and atmo-
813 spheric carbon dioxide forcing. *Nature* 486, 97–100.

814 Lawrence, K.T., Liu, Z., Herbert, T.D., 2006. Evolution of the Eastern Tropical
815 Pacific Through Plio-Pleistocene Glaciation. *Science* 312, 79–83. URL:
816 <https://science.sciencemag.org/content/312/5770/79>,
817 doi:10.1126/science.1120395. publisher: American Association for the
818 Advancement of Science Section: Research Article.

- 819 Lechler, A.R., Galewsky, J., 2013. Refining paleoaltimetry reconstructions of the
820 Sierra Nevada, California, using air parcel trajectories. *Geology* 41, 259–262.
- 821 Lisiecki, L.E., Raymo, M.E., 2005. A Pliocene-Pleistocene stack of 57 globally
822 distributed benthic $\delta^{18}\text{O}$ records. *Paleoceanography* 20.
- 823 Liu, J., An, Z., 2020. Leaf wax n-alkane carbon isotope values vary among ma-
824 jor terrestrial plant groups: Different responses to precipitation amount and
825 temperature, and implications for paleoenvironmental reconstruction. *Earth-*
826 *Science Reviews* 202, 103081.
- 827 Liu, J., Tian, J., Liu, Z., Herbert, T.D., Fedorov, A.V., Lyle, M., 2019.
828 Eastern equatorial Pacific cold tongue evolution since the late Miocene
829 linked to extratropical climate. *Science Advances* 5, eaau6060. URL:
830 <https://advances.sciencemag.org/content/5/4/eaau6060>,
831 doi:10.1126/sciadv.aau6060. publisher: American Association for the Ad-
832 vancement of Science Section: Research Article.
- 833 Menemenlis, S., Lora, J.M., Lofverstrom, M., Chandan, D., 2021. In-
834 fluence of stationary waves on mid-Pliocene atmospheric rivers and
835 hydroclimate. *Global and Planetary Change* 204, 103557. URL:
836 <https://linkinghub.elsevier.com/retrieve/pii/S0921818121001429>,
837 doi:10.1016/j.gloplacha.2021.103557.
- 838 Mix, H.T., Caves Rugeinstein, J.K., Reilly, S.P., Ritch, A.J., Winnick, M.J.,
839 Kukla, T., Chamberlain, C.P., 2019. Atmospheric flow deflection in the late

840 cenozoic sierra nevada. *Earth and Planetary Science Letters* 518, 76–85.
841 URL: <http://dx.doi.org/10.1016/j.epsl.2019.04.050>,
842 doi:10.1016/j.epsl.2019.04.050.

843 Munk, L., Chamberlain, C.P., 2011. Final technical report: G10ap00056-lithium
844 brine resources: A predictive exploration model. Research supported by the US
845 Geological Survey (USGS), Department of the Interior, under USGS award .

846 Munk, L.A., Hynek, S.A., Bradley, D.C., Boutt, D., Labay, K., Jochens, H., 2016.
847 Lithium Brines, a global perspective. Society of Economic Geologists. URL:
848 <http://dx.doi.org/10.5382/Rev.18.14>, doi:10.5382/rev.18.14.

849 Pascale, S., Boos, W.R., Bordoni, S., Delworth, T.L., Kapnick, S.B., Mu-
850 rakami, H., Vecchi, G.A., Zhang, W., 2017. Weakening of the North
851 American monsoon with global warming. *Nature Climate Change* 7, 806–
852 812. URL: <https://www.nature.com/articles/nclimate3412>,
853 doi:10.1038/nclimate3412.

854 Peuple, M.D., Bhattacharya, T., Lowenstein, T.K., McGee, D., Olson, K.J.,
855 Stroup, J.S., Tierney, J.E., Feakins, S.J., 2022. Biomarker and pollen evidence
856 for late Pleistocene pluvials in the Mojave Desert. *Paleoceanography and Pale-*
857 *oclimatology* 37, e2022PA004471.

858 Peuple, M.D., Bhattacharya, T., Tierney, J.E., Knott, J.R., Lowenstein, T.K.,
859 Feakins, S.J., 2024. Biomarker evidence for an MIS M2 Glacial-Pluvial
860 in the Mojave Desert before warming and drying in the late Pliocene.

- 861 Paleoclimatology and Paleoclimatology 39, e2023PA004687. URL:
862 <https://agupubs.onlinelibrary.wiley.com/doi/10.1029/2023PA004687>,
863 doi:10.1029/2023PA004687.
- 864 Pickart, R.S., Macdonald, A.M., Moore, G.W.K., Renfrew, I.A., Walsh,
865 J.E., Kessler, W.S., 2009. Seasonal Evolution of Aleutian Low Pres-
866 sure Systems: Implications for the North Pacific Subpolar Circula-
867 tion*. Journal of Physical Oceanography 39, 1317–1339. URL:
868 <http://journals.ametsoc.org/doi/10.1175/2008JPO3891.1>,
869 doi:10.1175/2008JPO3891.1.
- 870 Rousselle, G., Beltran, C., Sicre, M.A., Raffi, I., De Rafélis, M., 2013.
871 Changes in sea-surface conditions in the Equatorial Pacific during
872 the middle Miocene–Pliocene as inferred from coccolith geochem-
873 istry. Earth and Planetary Science Letters 361, 412–421. URL:
874 <https://www.sciencedirect.com/science/article/pii/S0012821X12006115>,
875 doi:10.1016/j.epsl.2012.11.003.
- 876 Sachse, D., Billault, I., Bowen, G.J., Chikaraishi, Y., Dawson, T.E., Feakins, S.J.,
877 Freeman, K.H., Magill, C.R., McInerney, F.A., Van Der Meer, M.T., et al.,
878 2012. Molecular paleohydrology: interpreting the hydrogen-isotopic composi-
879 tion of lipid biomarkers from photosynthesizing organisms. Annual Review of
880 Earth and Planetary Sciences 40, 221–249.
- 881 Sage, R.F., Wedin, D.A., Li, M., et al., 1999. The biogeography of c4 photosyn-
882 thesis: patterns and controlling factors. C4 plant biology 10, 313–376.

- 883 Sánchez-Montes, M.L., McClymont, E.L., Lloyd, J.M., Müller, J., Cowan, E.A.,
884 Zorzi, C., 2020. Late Pliocene Cordilleran Ice Sheet development with warm
885 northeast Pacific sea surface temperatures. *Climate of the Past* 16, 299–313.
- 886 Schrag, D.P., Hampt, G., Murray, D.W., 1996. Pore fluid constraints on the tem-
887 perature and oxygen isotopic composition of the glacial ocean. *Science* 272,
888 1930–1932.
- 889 Schumacher, C., Funk, A., 2023. Assessing Convective-Stratiform Precipitation
890 Regimes in the Tropics and Extratropics With the GPM Satellite Radar. *Geo-*
891 *physical Research Letters* 50, e2023GL102786.
- 892 Seki, O., Schmidt, D.N., Schouten, S., Hopmans, E.C., Damsté, J.S.S.,
893 Pancost, R.D., 2012. Paleoceanographic changes in the Eastern Equa-
894 torial Pacific over the last 10 Myr. *Paleoceanography* 27. URL:
895 <https://agupubs.onlinelibrary.wiley.com/doi/abs/10.1029/2011PA002158>,
896 doi:<https://doi.org/10.1029/2011PA002158>. eprint:
897 <https://agupubs.onlinelibrary.wiley.com/doi/pdf/10.1029/2011PA002158>.
- 898 Shaari, H.b., Yamamoto, M., Irino, T., 2013. Enhanced upwelling
899 in the eastern equatorial Pacific at the last five glacial terminations.
900 *Palaeogeography, Palaeoclimatology, Palaeoecology* 386, 8–15. URL:
901 <https://www.sciencedirect.com/science/article/pii/S0031018213001600>,
902 doi:10.1016/j.palaeo.2013.03.022.
- 903 Teng, F.Z., McDonough, W., Rudnick, R., Dalpé, C., Tomascak, P., Chappell,

904 B., Gao, S., 2004. Lithium isotopic composition and concentration of the up-
905 per continental crust. *Geochimica et Cosmochimica Acta* 68, 4167–4178. URL:
906 <https://www.sciencedirect.com/science/article/pii/S0016703704004326>,
907 doi:<https://doi.org/10.1016/j.gca.2004.03.031>.

908 Thompson, R.S., 1991. Pliocene environments and climates in the western United
909 States. *Quaternary Science Reviews* 10, 115–132.

910 Tierney, J.E., Haywood, A.M., Feng, R., Bhattacharya, T., Otto-Bliesner, B.L.,
911 2019. Pliocene warmth consistent with greenhouse gas forcing. *Geophysical*
912 *Research Letters* 46, 9136–9144.

913 Tierney, J.E., Pausata, F.S., deMenocal, P.B., 2017. Rainfall regimes of the Green
914 Sahara. *Science advances* 3, e1601503.

915 Tierney, J.E., Tingley, M.P., 2018. BAYSPLINE: A new calibration for the
916 alkenone paleothermometer. *Paleoceanography and Paleoclimatology* 33, 281–
917 301.

918 Vine, J.D., 1975. Lithium in sediments and brines-how, why, and where to search.
919 *Journal of Research of the US Geological Survey* 3, 479–485.

920 Wallace, B., Minder, J.R., 2024. The North American Mon-
921 soon precipitation response to climate warming at convection-
922 permitting scales. *Climate Dynamics* 62, 497–524. URL:
923 <https://link.springer.com/10.1007/s00382-023-06920-6>,
924 doi:[10.1007/s00382-023-06920-6](https://doi.org/10.1007/s00382-023-06920-6).

- 925 Wang, L., Hu, H., Yang, X., 2019. The atmospheric responses
926 to the intensity variability of subtropical front in the winter-
927 time North Pacific. *Climate Dynamics* 52, 5623–5639. URL:
928 <http://link.springer.com/10.1007/s00382-018-4468-9>,
929 doi:10.1007/s00382-018-4468-9.
- 930 Westerhold, T., Marwan, N., Drury, A.J., Liebrand, D., Agnini, C., Anagnostou,
931 E., Barnet, J.S., Bohaty, S.M., De Vleeschouwer, D., Florindo, F., et al., 2020.
932 An astronomically dated record of Earth’s climate and its predictability over the
933 last 66 million years. *Science* 369, 1383–1387.
- 934 Williams, A.P., Cook, E.R., Smerdon, J.E., Cook, B.I., Abatzoglou, J.T., Bolles,
935 K., Baek, S.H., Badger, A.M., Livneh, B., 2020. Large contribution from an-
936 thropogenic warming to an emerging North American megadrought. *Science*
937 368, 314–318.
- 938 Windler, G., Tierney, J.E., deMenocal, P.B., 2023. Hydroclimate Variability in the
939 Equatorial Western Indian Ocean for the Last 250,000 Years. *Paleoceanography*
940 and *Paleoclimatology* 38, e2022PA004530.
- 941 Yamamoto, M., Kobayashi, D., 2016. Surface ocean cooling in the subarctic North
942 Pacific during the late Pliocene suggests an atmospheric reorganization prior to
943 extensive Northern Hemisphere glaciation. *Deep Sea Research Part II: Topical*
944 *Studies in Oceanography* 125, 177–183.

Supporting Information for “Great Basin hydroclimate modulated by Pacific temperature gradients over the Plio-Pleistocene transition”

Tripti Bhattacharya¹, Peter R. Brennan¹, Daniel E Ibarra², Catherine A.

Gagnon², Kristina L. Butler², Alexa Terrazas⁶, Shaw Miller², Lee Ann

Munk³, David F. Boutt⁴, Ran Feng⁵, Stephanie N. Bullinger¹, Lucy

Weisbeck¹

¹Department of Earth and Environmental Sciences, Syracuse University, Syracuse NY

²Department of Earth, Environmental and Planetary Science, Brown University, Providence, RI

⁶Department of Atmospheric and Ocean Sciences, University of California Los Angeles, Los Angeles, CA

³Department of Geological Sciences, University of Alaska-Anchorage, Anchorage, AK

⁴Department of Geosciences, University of Massachusetts-Amherst, Amherst, MA

⁵Department of Geosciences, University of Connecticut, Storrs, CT

Contents of this file

1. Figures S1 to S3
2. References

Figures

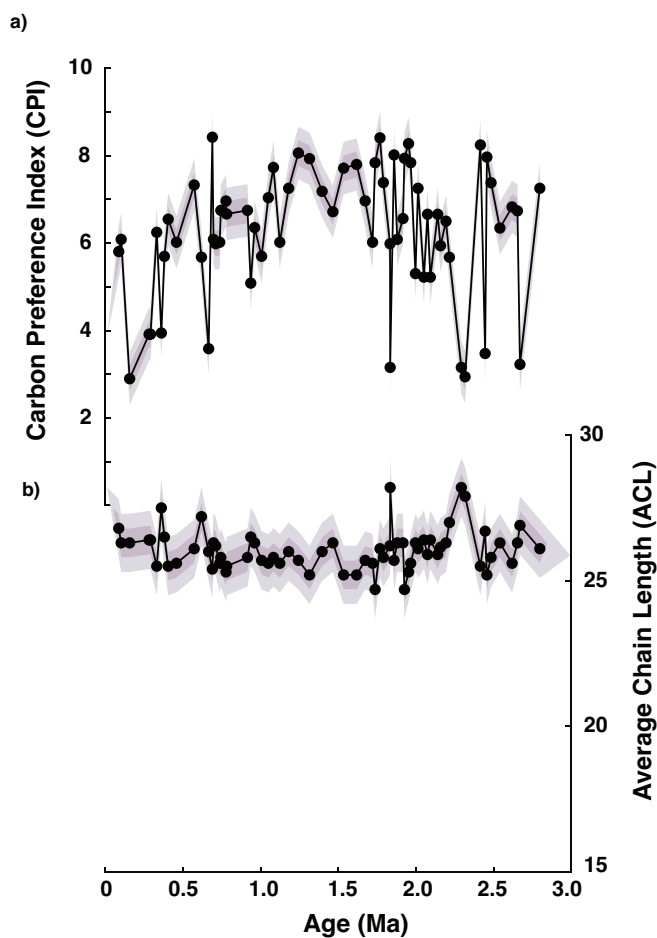


Figure S1. Average chain length (panel a) and carbon preference index (panel b) for alkanolic acids in Clayton Valley record.

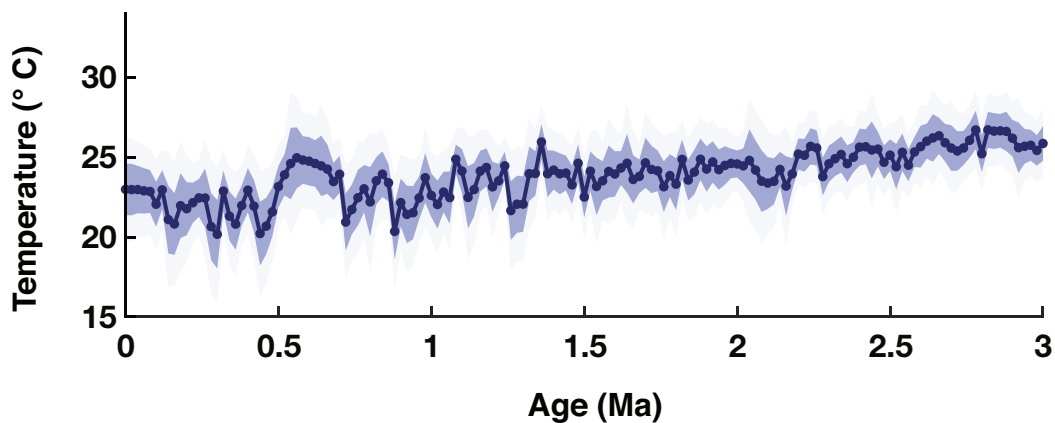


Figure S2. Evolution of temperature in the eastern equatorial Pacific cold tongue between the early Pliocene. For more details on the calculation method, please see (Bhattacharya et al., 2022).

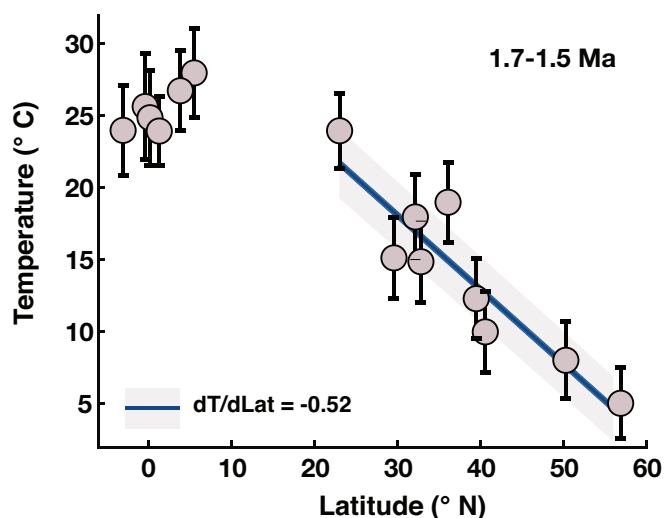


Figure S3. Pacific extratropical meridional temperature gradient between 1.5 and 1.7 Ma. A least-squares regression line is calculated between 20 and 60 ° N to visualize the slope of this temperature gradient. See Figure 6 in main text for SST gradients at 2.8 and 2.4 Ma respectively. For more information on the SST proxy compilation, see the main text.

References

- Bhattacharya, T., Feng, R., Tierney, J. E., Rubbelke, C., Burls, N., Knapp, S., & Fu, M. (2022). Expansion and intensification of the north american monsoon during the pliocene. *AGU Advances*, 3(6), e2022AV000757.